The prediction of flow pattern maps in minichannels

Article *in* Multiphase Science and Technology · January 2007

DOI: 10.1615/MultScienTechn.v19.i1.20

2 authors:

Amos Ullmann
Tel Aviv University
131 PUBLICATIONS **2,976** CITATIONS

SEE PROFILE

Neima Brauner
Tel Aviv University
293 PUBLICATIONS **5,780** CITATIONS

SEE PROFILE

Multiphase Science and Technology, Vol. 19, No. 1, pp. 49–73, 2007

THE PREDICTION OF FLOW PATTERN MAPS IN MINICHANNELS

Amos Ullmann and Neima Brauner
Dept. of Fluid Mechanics and Heat Transfer, School of Mechanical Engineering, Faculty of Engineering, Tel-Aviv University, Tel-Aviv, Israel

Abstract. Commonly used models for predicting the flow patterns and flow pattern transitions are established for gas-liquid flows in normal-size channels ($D > 0.5''$). Those are generally found to predict poorly experimental two-phase flow pattern data in minichannels. In this study, the effect of the channel diameter on the mechanisms leading to flow pattern transitions are reexamined in an attempt to identify the governing phenomena involved in two-phase flow in small-diameter channels. Accordingly, appropriate mechanistic models are suggested and compared with experimental flow pattern maps available from the literature. These models also indicate the controlling dimensionless groups and the critical values associated with the various flow pattern transitions. The analyses also suggest criteria, in terms of dimensionless Eotvos number, Eo_D, that indicate when the conventional models must be substituted with the minichannel models. The reasons for the disappearance of the stratified flow in mini- and microchannels are elaborated, and the various mechanisms leading to the establishment of annular flow as the basic flow pattern in low Eo_D systems are discussed.

1. INTRODUCTION

The miniaturization of engineering systems requires the establishment of design tools for two-phase flow in mini- and microchannels. The prediction of two-phase flow pattern and the associated transport phenomena in minichannels has become important for the design of many applications in chemical and material process engineering, in cooling of electric power and laser devices, in nuclear reactors, and for the medical and biotechnology systems. The interest in minichannels has manifested in an increasing number of publications on adiabatic gas-liquid flows and on boiling and condensation phenomena in mini- and microchannels (*e.g.*, Suo and Griffith 1964, Damianides and Westwater 1988, Barnea *et al.* 1983, Buiswas and Greenfield 1985, Brauner 1990, Brauner and Moalem Maron 1992, Barajas and Panton 1993, Fukano and Kariyasaki 1993, Wilmarth and Ishii 1994, Triplett *et al.* 1999, Serizawa *et al.* 2002, Kew and Cornwell 1997, Chen *et al.* 2002, Hetstroni *et al.* 2005). The state of the art in the field has been summarized in several extensive review articles (*e.g.*, Ghiaasiaan and Absel-Khalik 2001, Watel 2003, Cheng and Mewes 2006, Thome 2006).

The commonly used models for predicting the flow patterns and flow pattern transition were established mainly based on theory and observations that are relevant to gas-liquid flows in pipe diameters ranging from 0.5″ to 5″. Those models, and the corresponding flow pattern maps, are generally found to predict poorly experimental two-phase flow pattern data in minichannels. This is attributed mainly to the increased role of surface tension and wetting effects associated with reducing the channel size. Therefore downscaling of the models and design tools developed for two-phase flow in normal-size channels may lead to erroneous results.

Different classifications for channel sizes have been suggested in the literature. In heat exchanger engineering, the common practice is to set the threshold value for conventional channels at hydraulic pipe diameter of $D_h = 6$ mm, and compact heat exchangers are those having a channel size between 1 and 6 mm (Mehendale *et al.* 2000). Kandlikar (2001, 2002) examined a wider range of applications and extended the range of conventional channels to $D_h > 3$ mm, and minichannels are those in the range of 200 μm $< D_h <$ 3 mm. However, any dimensional cutoff value cannot be expected to be representative for a variety of two-phase flow systems of different fluid properties. In two-phase flow, the dimensionless system Eotvos number, $\mathrm{Eo}_D = \Delta\rho g D^2/8\sigma$, has been found to be important in channel size classification. It represents the ratio between gravity and surface tension forces.

The threshold value set on the Eo_D depends on the physical phenomenon examined and varies in the range of 0.04–5. In small Eo_D systems, the bubble/drop drift is negligible, even in vertical systems (Suo and Griffith 1964; Zukoski 1966), and the flow patterns in gas-liquid systems resemble those obtained with conventional channel sizes under microgravity conditions or in liquid-liquid systems of similar phase density (Brauner 1990, Brauner and Moalem Maron 1992). Fluid/wall wetting characteristics become important (Buiswas and Greenfield 1985, Barajas and Panton 1993, Brauner *et al.* 1996a, Gorelik and Brauner 1999, Brauner *et al.* 1998), and the boiling phenomena differ from those obtained in large Eo_D systems (Kew and Cornwell 1997).

In this study, we examine the classification of the channel size from the viewpoint of flow patterns and their transition boundaries. As a test case, we take the experimental flow pattern map reported by Triplett *et al.* (1999) for air-water flow in 1.097-mm Pyrex pipe corresponding to $Eo_D = 0.021$. This test case was selected as the flow pattern map was complemented with photographs showing the various flow patterns observed in the experiments, which are important for substantiating the flow pattern classification.

The flow patterns identified are shown in Fig. 1 and are similar to those observed also in normal-size pipes: bubbly flow, slug flow, churn (aerated slugs) flow, and annular flow. This flow pattern map was shown to be in reasonable agreement with other studies of air-water flow in a similar pipe diameter range (Ghiaasiaan and Absel-Khalik 2001). However, as shown by Triplett *et al.* (1999), the application of models developed for normal-size pipes failed to predict the flow patterns boundaries. Therefore, in the present study, the models are reexamined and revised to identify the mechanisms and the associated controlling dimensionless parameters that determine the flow pattern transitions in such small-diameter pipes.

The models used yield the boundaries depicted in Fig. 1, which are in reasonable agreement with the data. The reasons for the disappearance of the stratified flow in mini- and microchannels are elaborated, and the various mechanisms leading to

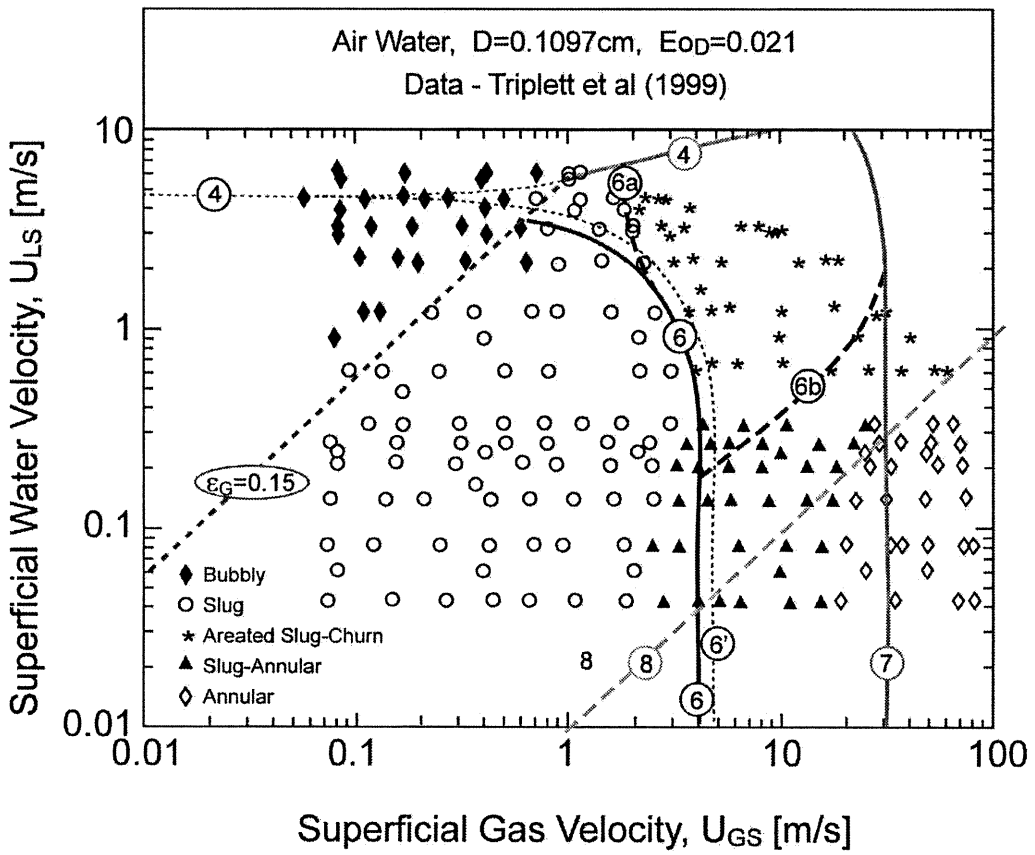

Figure 1 Flow pattern map in horizontal 1-mm pipe: experimental data (Triplett *et al.* 1999) and predicted boundaries (present study).

the establishment of annular flow as the basic flow pattern in low-Eo_D systems are discussed.

2. BUBBLY TO PLUG FLOW TRANSITION

In low-Eo_D systems, the basic flow pattern at low gas flow rates is the bubbly flow, with the liquid (the wetting phase) being the continuous phase. This is similar to gas-liquid flow in vertical, normal-size pipes. However, the bubble slip is negligible in small Eo_D systems (Suo and Griffith 1964, Zukoski 1966). A simplified model for the transition from bubbly flow with spherical bubbles to elongated bubbles (plug flow, denoted in Triplett *et al.* (1999) as slug flow) can be obtained based on geometrical considerations (see inserted pictures b and d in Fig. 3). The critical holdup for coalescence of spherical bubbles to form elongated bubbles is estimated based on the void fraction of a train of contacting bubbles with a diameter of about half of the pipe diameter (see Fig. 2). This corresponds to a gas void fraction of $(\varepsilon_G)_{\text{crit}} = 0.166$. As the slip between the phases is negligible, the relation between the phases' superficial velocities, U_{LS} and U_{GS}, is given by

$$U_{LS} = \frac{1 - (\varepsilon_G)_{\text{crit}}}{(\varepsilon_G)_{\text{crit}}} U_{GS} \tag{1}$$

The line drawn in Fig. 3 was obtained with $(\varepsilon_G)_{\text{crit}} = 0.15$, which is shown to represent reasonably the experimentally observed transition.

It is worth noting that in the experimental flow pattern map, no distinction was made between bubbly flow and dispersed bubble flow. These two flow patterns typically differ in their characteristic bubble size and, consequently, in the associated transport phenomena. Therefore the identification of this transition is of importance. Pictures taken by Triplett *et al.* (1999) in the same system suggest that such a transition actually takes place within the reported operational flow rates (see inserted pictures in Fig. 3). Obviously, the flow pattern in the inserted picture a is significantly different from that indicated by b, and also from that shown in c. Note that pictures a and c correspond to almost the same U_{GS} and very close U_{LS}. While the flow pattern in c may still be classified as bubbly flow, that in a, in which the bubble size is much smaller, should be classified as dispersed bubble flow.

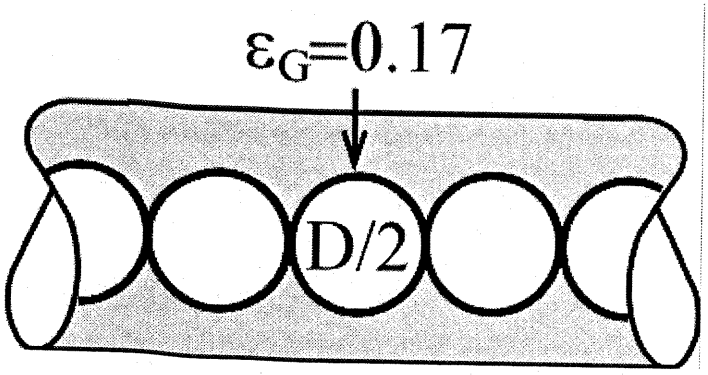

Figure 2 Schematic of a train of contacting bubbles.

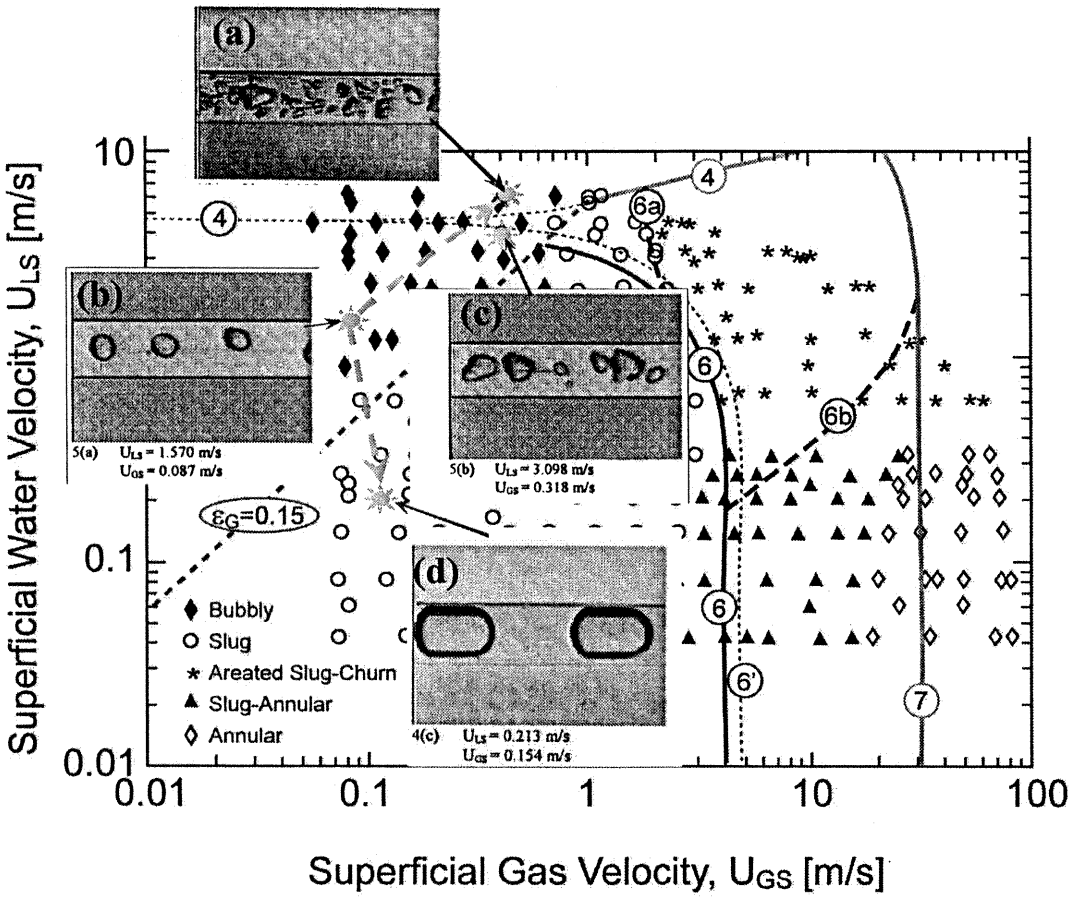

Figure 3 Transition to homogeneous dispersed bubble flow (boundary 4).

3. TRANSITION TO DISPERSED BUBBLE FLOW

The mechanism leading to the establishment of homogeneous dispersion of bubbles is attributed to bubble breakage due to turbulence in the continuous phase, as suggested by Hinze (1955). Its application to the prediction of dispersed flow boundaries in gas-liquid and liquid-liquid systems was presented in Brauner (2001) and is briefly reviewed herein.

The basic idea is that this transition occurs when the turbulence in the continuous phase is sufficiently high to disperse the other phase into stable spherical droplets/bubbles. Their maximal drop size, $d_{\max}$, should then be small compared to a critical size d_{crit} of coalescing droplets/bubbles, $d_{\max} \leq d_{\text{crit}}$. The maximal droplet/bubble size for dilute dispersion, $(d_{\max})_o$, is estimated based on a force balance between the momentum exerted by the turbulent eddy and the surface tension stabilizing force.

In dense dispersion of coalescing droplets/bubbles, the maximal drop size $(d_{\max})_\varepsilon$ is estimated based on an energy balance, comparing the flux of turbulent energy in the continuous phase and the flux of surface energy generated in the recurrently renewed dispersion. The maximal droplet/bubble size in the system is taken as the larger value

of these two estimates. Obviously, the modeling of $d_{\max}$ requires the modeling of the turbulence intensity in the continuous phase.

The critical size of coalescing droplet/bubble is taken as the minimal size between the following three characteristic values: $d_{c\sigma}$, which represents the size of deformable droplet/bubble; d_{cb} for floating droplet/bubble due to buoyant forces (in horizontal/slightly inclined pipes) that overcome the dispersing forces due to the turbulent eddies' momentum; and a value that is of the order of pipe diameter (say, $0.5D$). Accordingly, the transitional criterion is stated as

$$d_{\max} = \max\{(d_{\max})_o, (d_{\max})_\varepsilon\} \leq d_{\text{crit}} = \min\{d_{c\sigma}, d_{cb}, 0.5D\} \tag{2}$$

where

$$d_{c\sigma} = \sqrt{\frac{0.4\sigma}{\Delta\rho g \cos\beta'}} \tag{3a}$$

$$d_{cb} = \frac{27}{2} D \frac{\rho_c}{\Delta\rho} f^2 \mathrm{Fr}_c^3; \quad d_{\max} \leq 0.1D; \quad \mathrm{Fr}_c = \frac{U_m^2}{Dg\cos\beta} \tag{3b}$$

$$d_{cb} = \frac{3}{8} D \frac{\rho_c}{\Delta\rho} f\,\mathrm{Fr}_c; \quad d_{\max} > 0.1D \tag{3c}$$

U_m is the mixture velocity ($U_m = U_{cs} + U_{ds}$), f is the Reynolds-dependent wall friction factor ($f = f(\mathrm{Re}_c)$), β is the pipe inclination angle, and β' is defined as

$$\beta' = \begin{cases} |\beta|; & |\beta| < 45^\circ \\ 90 - |\beta|; & |\beta| > 45^\circ \end{cases} \tag{3d}$$

Note that the first model for d_{cb} (Eq. (3b)) is applicable in large-diameter tubes, where $d_{\max} < 0.1D$ and homogeneous turbulence can be assumed; otherwise, Eq. (3c), the turbulent velocity, is estimated based on the shear velocity (see Table 1). The other relevant dimensionless parameters are the following:

$$\begin{aligned} \mathrm{We}_c &= \frac{\rho_c D U_m^2}{\sigma} & \mathrm{Re}_c &= \frac{\rho_c D U_m}{\mu_c} \\ \varepsilon_d &= \frac{Q_d}{Q_c + Q_d} & \mathrm{Eo}_D &= \frac{D^2 \Delta\rho g \cos\beta'}{8\sigma} \end{aligned} \tag{4}$$

Here subscript c denotes the continuous phase (liquid) and subscript d the dispersed (gas) phase.

Table 1 summarizes the various models for $d_{\max}$ and their applicability range. The H-model, which is an extension of the Hinze (1955) model, assumes homogenous turbulence, where the turbulent velocity u' is related to the turbulent energy dissipation $\bar{e}$. This model is valid for droplets/bubbles smaller than $0.1D$, hence for $\mathrm{Eo}_D > 5$. For smaller Eo_D, the turbulent velocity is modeled by the frictional velocity, u^*, and $d_{\text{crit}} = d_{c\sigma}$ (as $d_{cb} > d_{c\sigma}$). The resulting K-model is valid for $d_{\max} < 0.5D$, hence $0.2 < \mathrm{Eo}_D < 5$. For $\mathrm{Eo}_D < 0.2$ (smaller tubes), where the critical droplet/bubble size is constrained by the pipe diameter (taken as $d_{\text{crit}} = 0.5D$), the K1-model is applicable.

Table 1 Models for droplet/bubble size for the prediction of boundary 4.

Model	Applicability range	$\tilde{d}_{\max}$	$\tilde{d}_{\text{crit}}$
H-model	$\tilde{d}_{\max} < 0.1$ $\downarrow$ $\text{Eo}_D > 5$	Homogeneous turbulence: $u'^2 = 2(\bar{\varepsilon}\, d_{\max})^{2/3}$ $\tilde{d}_{\max} = C_H(\varepsilon_d)\text{We}_c^{-0.6}\text{Re}_c^{0.08}$	$\tilde{d}_{c\sigma}$ $\tilde{d}_{cb}$ Horizontal/slightly inclined
K-model	$0.1 < \tilde{d}_{\max} < 0.5$ $\downarrow$ $0.2 < \text{Eo}_D < 5$	Turbulence model: $u' = u^* = \sqrt{\tau_c/\rho_c}$ $\tilde{d}_{\max} = C_K(\varepsilon_d)\text{We}_c^{-1}\text{Re}_c^{0.2}$	$\tilde{d}_{c\sigma}$
K1-model	$\text{Eo}_D < 0.2$	Turbulence model: $u' = u^* = \sqrt{\tau_c/\rho_c}$ $\tilde{d}_{\max} = C_K(\varepsilon_d)\text{We}_c^{-1}\text{Re}_c^{0.2}$	0.5
$\text{Re}_c > 2100$	Critical velocity constrained by transition to turbulent flow		

It is worth emphasizing that all these models are relevant only for turbulent flow in the continuous phase and therefore are constrained by the condition that $\text{Re}_c > 2100$. Note that in the case of dispersed bubble flow, the continuous phase (c) is the liquid (L), and the dispersed phase (d) is the gas (G).

The minimal mixture velocity U_m required for the transition to dispersed bubble flow versus the tube diameter (or the Eo_D) in the air-water system is demonstrated in Fig. 4. It evolves by applying the various models shown in Table 1 in their applicability range. As shown, large-diameter pipes correspond to $\text{Eo}_D > 100$, where the critical mixture velocity increases with the tube diameter ($U_m \propto D^{0.43}$). In this region, the applicable model is independent of the pipe inclination.

For lower Eo_D, some differences exist between the critical mixture velocities predicted for horizontal and vertical systems. However, in the range of small-diameter tubes, where the K1-model is applicable, the trend of the dependence of U_m on the tube diameter changes compared to that predicted for large diameters. The transitional criteria of the K1-model (for liquid as the continuous phase and gas as the dispersed phase) read

$$\left(\tilde{d}_{\max}\right)_o = \frac{d_{\max}}{D} = 30\text{We}_L^{-1}\text{Re}_L^{0.2} \leq 0.5 \tag{5}$$

$$\left(\tilde{d}_{\max}\right)_\varepsilon = \frac{d_{\max}}{D} = 174 C_K \text{We}_L^{-1}\text{Re}_L^{0.2}\frac{\varepsilon_G}{1-\varepsilon_G} \leq 0.5,\ C_K \approx O(1) \tag{6}$$

In this model, the minimal critical U_m increases with reducing the pipe diameter ($U_m \propto D^{-0.44}$). The test case of D = 1.097 mm shown in Fig. 3 corresponds to this

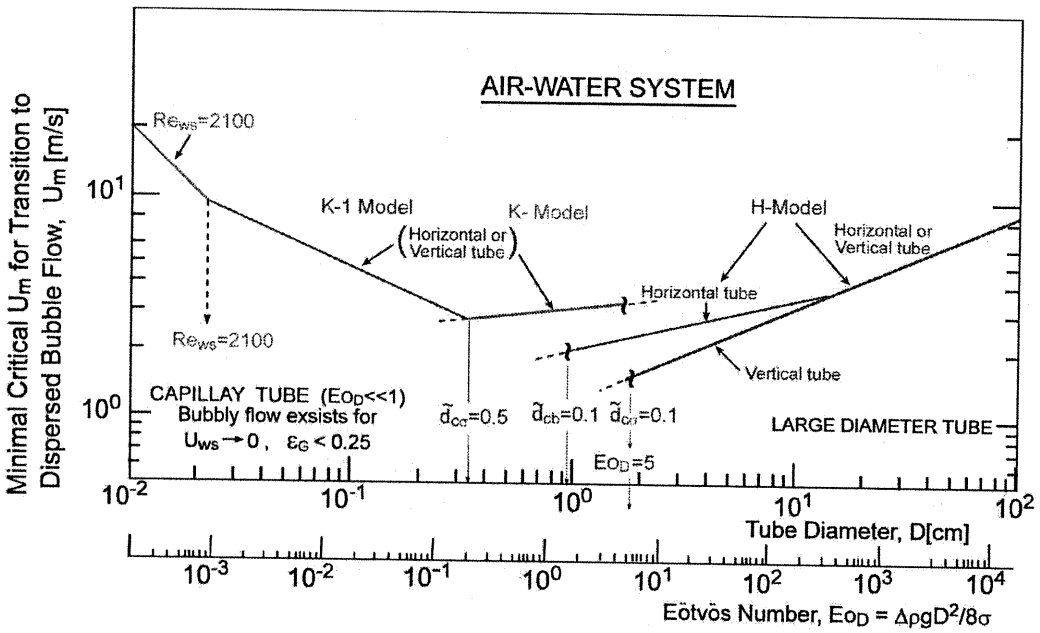

Figure 4 Minimal mixture velocity for the transition to dispersed bubble flow in air-water systems (boundary 4).

region. The predicted boundary is indicated by line 4 in the figure. If the pipe diameter is further reduced below 200 μm, the critical U_m is constrained by the transition to turbulent flow ($U_m \propto D^{-1}$).

The concave shape of the critical U_m versus D (Fig. 4) suggests that similar critical conditions can be experimentally observed in considerably different diameters. However, such experimental observation should not be interpreted as independent of the transition to dispersed bubble flow on the channel diameter.

4. TRANSITION TO AERATED SLUGS (CHURN) FLOW

Picture b (inserted in Fig. 5) demonstrates the flow pattern classified by Triplett *et al.* (1999) as churn flow. However, the flow structure in the picture actually appears as aerated slugs. Two possible models for predicting the transition to aerated slugs are tested. The first is denoted as the Slug Bulk (SLB) model, which is based on the idea suggested by Barnea and Brauner (1985). The second model is based on the Taylor bubble wake (TBW) model presented in Ullmann and Brauner (2004).

The SLB model attributes the slug aeration to the bubble breakage due to turbulence in the liquid slug bulk (where the liquid velocity is the mixture velocity, $U_L = U_m$). The flow in the liquid slug, and the breakage mechanism, is considered to be the same as that prevailing in the dispersed-bubble/slug boundary under conditions of the same mixture velocity. Therefore the critical mixture velocity for the onset of slug aeration, $(U_m)_{\text{crit}}$, corresponds to the minimal critical mixture velocity for the transition to dispersed bubble flow. It also represents the superficial liquid velocity along boundary 4 in the limit of $U_{GS} \rightarrow 0$ (see Fig. 3).

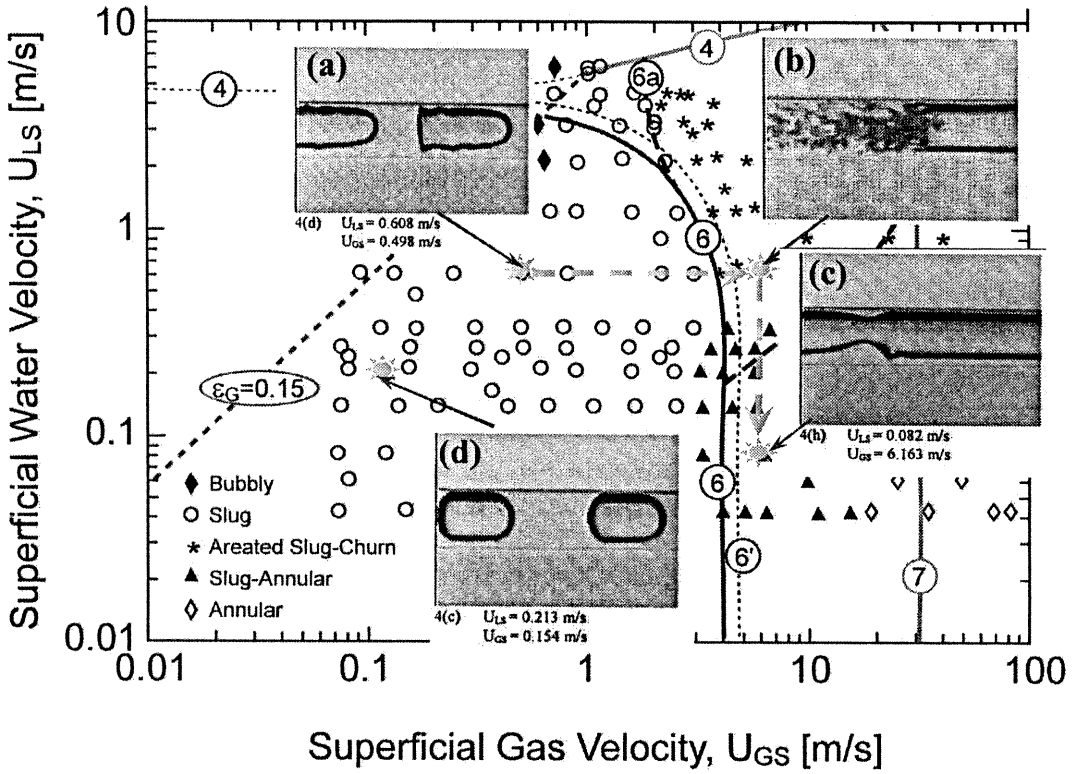

Figure 5 Transition between slug and aerated slug (churn?) flows (boundary 6).

Table 2 summarizes the models for $(U_m)_{\text{crit}}$ for the various range of Eo_D and the predicted void fraction in the liquid slug (ε_{LS}) for $U_m > (U_m)_{\text{crit}}$. The studied test case corresponds to the K1-model, whereby the transition to aerated slugs is depicted by line 6′ (Fig. 5), which is obtained by

$$(U_m)_{\text{crit}} = (U_{GS} + U_{LS})_{\text{crit}} = 9.72 \frac{\sigma^{0.55}}{\rho_L^{0.44} \mu_L^{0.11} D^{0.44}} \tag{7}$$

The second (TBW) model attributes the slug aeration to fragmentation of the elongated (Taylor, TB) bubbles due to the turbulence in the TB wake. In the wake region, the turbulent field is dominated by the shear layer formed between the liquid film (moving at a velocity U_{Lf}), which is penetrating into the faster slug bulk. Generally, since the calculation of U_{Lf} is coupled with other slug flow variables, the application of the TBW model requires a complete model for slug flow. However, in systems of $\text{Eo}_D < 0.2$, the TB slip is negligible, and consequently, $|U_{Lf}| \ll |U_m|$. Under such conditions, the TBW model results in the following expression for the critical mixture velocity for slug aeration:

$$(U_m)_{\text{crit}} = (U_{GS} + U_{LS})_{\text{crit}} = 16 \left[\frac{\sigma}{\rho_L D} \right]^{0.5} \tag{8}$$

It corresponds to a critical Weber number

Table 2 Aerated slug boundary (6′): SLB model ($C_H, C_K = o(1)$ tuned constant)

Eo_D	ε_{LS} for $U_m > (U_m)_{crit}$	$(U_m)_{crit}$
$Eo_D > 5$, H-model	$\frac{0.022C_H^{-1}We_L f_L^{2/3}(Eo_D \cos\beta')^{-5/6}}{1+0.022C_H^{-1}We_L f_L^{2/3}(Eo_D \cos\beta')^{-5/6}}$	$2.65\left\{\frac{(\lvert\Delta\rho\rvert g\cos\beta')^{0.5}\sigma^{0.1}D^{0.48}}{\rho_L^{0.52}\mu_L^{0.08}}\right\}^{0.893}$
$0.2 < Eo_D < 5$, K-model	$\frac{0.028C_K^{-1}We_L f_L(Eo_D \cos\beta')^{-0.5}}{1+0.028C_K^{-1}We_L f_L(Eo_D \cos\beta')^{-0.5}}$	$8.53\left\{\frac{(\sigma\Delta\rho g\cos\beta')^{0.5}D^{0.2}}{\rho_L^{0.8}\mu_L^{0.2}}\right\}^{0.55}$
$Eo_D < 0.2$, K1-model	$\frac{0.25C_K^{-1}We_L f_L}{1+0.25C_K^{-1}We_L f}$	$9.72\left(\frac{\sigma}{\rho_L^{0.8}\mu_L^{0.2}D^{0.8}}\right)^{0.55}$

$$(We_m)_{crit} = \frac{\rho_L(U_{GS}+U_{LS})^2 D}{\sigma} = 256 \tag{9}$$

This boundary is indicated in Fig. 5 by boundary 6. Comparison of Eqs. (7) and (8) shows that both models yield similar results in terms of the dependence on tube diameter, liquid density, and surface tension (the former indicates a mild dependence on the liquid viscosity). As shown in Fig. 5, both models practically predict the same critical conditions for the air-water system. Their application is restricted to conditions where the flow in the liquid slug is turbulent ($Re_L = \rho_L D U_m/\mu_L > 2100$). Otherwise, if conditions (7) or (8) correspond to $Re_L < 2100$, boundary 6 becomes constrained by the critical Re_L.

It is worth recalling that in several publications reporting flow patterns observed in small-diameter channels and in microgravity conditions (Rezkallah 1996, Lowe and Rezkallah 1999), it has been suggested that the critical conditions for transition to frothy slug-annular flow can be empirically correlated in terms of a critical gas phase Weber number, $(We_G)_{crit} = \rho_G U_{GS}^2 D/\sigma \approx 1 \div 5$. On the other hand, the TBW model, Eq. (9), suggests that the critical conditions correspond to a critical Weber number of the liquid slug. Indeed, at high U_{GS}(and relatively low U_{LS}) along boundary 6, the velocity in the slug is practically equal to U_{GS}. However, Eq. (9) suggests a critical We that is based on the liquid density, rather than on the gas density, and consequently, it corresponds to a larger critical value than that suggested for $(We_G)_{crit}$.

Inspection of Fig. 5 shows that although the models predict that the region right of boundaries 6 and 6′ should correspond to aerated slugs, the observed flow pattern for relatively low liquid superficial velocities is slug annular. It is characterized with large waves that almost block the slug passage (see inserted picture c). This observation may be a result of the length of the pipe used in the experimental setup (L_{pipe} = 0.3 m). Applying the complete slug flow model (Brauner and Ullmann 2004) in this region indicates that below boundary 6b, the length of the shortest elongated bubble (which is associated with the shortest possible liquid slug length, $1D$) is already longer than the experimental pipe. This implies that with longer pipes, the region of aerated slugs could be larger and extend to lower liquid superficial velocities (below boundary 6b).

Similarly, for high U_{LS}, left of boundary 6a, the slug flow model indicates that aerated slugs are obtained only for fully developed, long liquid slugs (length greater than $22D$) and long TB, which may not have been obtained in the short pipe. This may be the reason that the observed flow pattern in this region was slug (rather than aerated slug) flow.

5. TRANSITION TO BULLET-SHAPED BUBBLES

Figure 5 shows two pictures (a, d) of the elongated bubble observed within the slug flow region. However, examining these tow pictures indicates that the bubbles differ significantly in their shapes. While in those corresponding to relatively low flow rates, the bubble nose and tail are curved, whereas at higher flow rates (d), the bubble acquires a bullet shape with a flat tail (a). In small-diameter tubes, the surface tension force can overcome the inertial force of the following liquid slug, which, in large-diameter tubes, results in a flat tail. Thus a rough criterion for the conditions where a curved bubble tail can be maintained may be represented by

$$\frac{4\sigma}{D} \geq \frac{1}{2}\rho_L U_L^2 \tag{10}$$

Since the velocity of the liquid slug is the mixture velocity ($U_L = U_{GS} + U_{LS} = U_m$), the transition criterion corresponds to a critical Weber number of the liquid slug:

$$(\mathrm{We}_m)_{\mathrm{crit}} = \frac{\rho_L U_m^2 D}{\sigma} = 8 \quad \mathrm{Re}_{L,G} < 2100 \tag{11}$$

It can be argued that such a simple criterion holds only in laminar flow in the phases; as in turbulent flow, the inertia of turbulent eddies should also be considered. Criterion (11) is depicted in Fig. 6 as boundary 3.

6. TRANSITION TO ANNULAR FLOW

The transition to annular flow in horizontal or slightly inclined gas-liquid systems can be attributed to one of the following mechanisms.

6.1 *Loss of stability of the stratified flow structure*

The instability is due to the Kelvin-Helmholtz (KH) mechanism. In many studies (*e.g.*, Taitel and Dukler 1976, Brauner and Moalem Maron 1991, 1993), it has been suggested that the critical gas velocity for transition to annular flow can be predicted by the threshold value where the transient model equations for the stratified flow become ill posed (also denoted as the inviscid KH stability criterion). For thin liquid layers (low U_{LS} and $\varepsilon_G \approx 1$), the corresponding critical U_{GS} is given by (Brauner and Moalem Maron 1991)

$$U_{GS} \geq C_1 \left[\frac{D\Delta\rho g \cos\beta + D\sigma k^2}{\rho_G}\right]^{0.5} \tag{12}$$

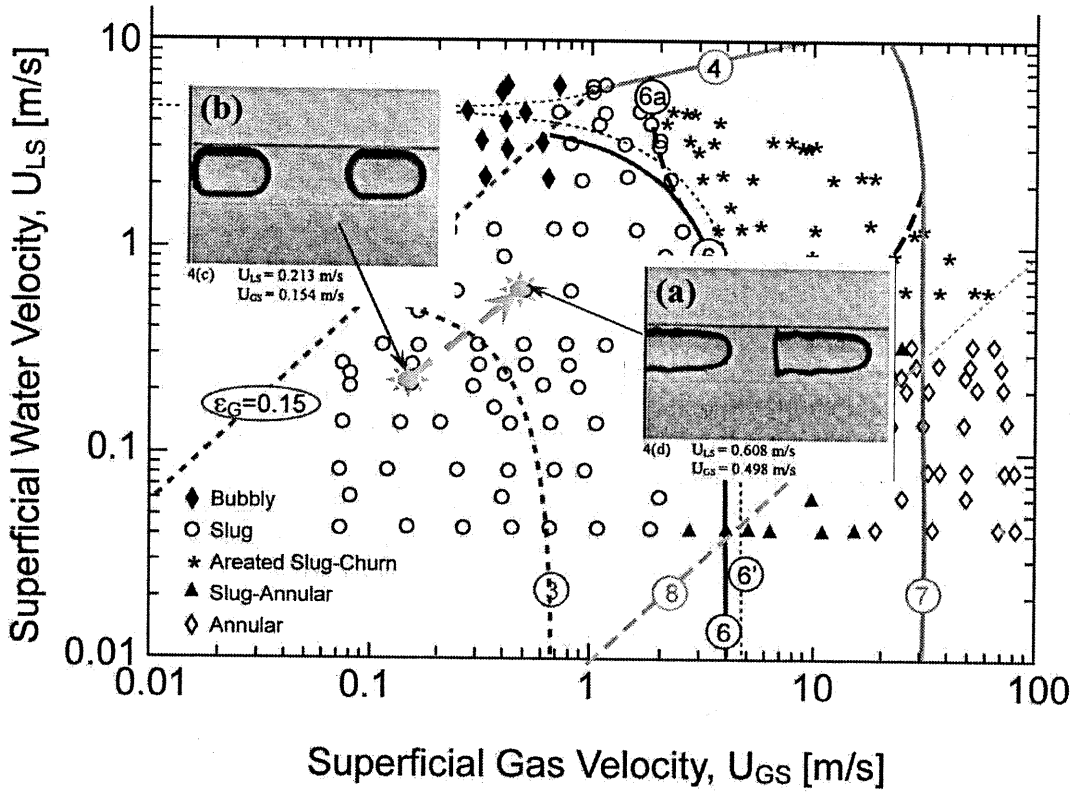

Figure 6 Elongated–bullet-shaped bubble transition (boundary 3).

where k is the typical long wave number, $k \approx 2\pi/D$ (Brauner and Moalem Maron 1992), and C_1 is a geometrical constant. In rectangular conduits, $C_1 = 1$, whereas in pipe flow, it varies with the liquid layer thickness, $\tilde{h} = h/D$ (for thin layers, $C_1 \approx 0.63\tilde{h}^{-0.25}$).

The criterion given in Eq. (12) implies that for large Eo_D systems ($\mathrm{Eo}_D > 5$), the critical gas velocity is scaled with $(D\Delta\rho g \cos\beta/\rho_G)^{0.5}$ and thus increases proportionally to $D^{0.5}$ and corresponds to a critical gas Froude number, $\mathrm{Fr} = \frac{\rho_G}{\Delta\rho}\frac{U_{GS}^2}{Dg\cos\beta} \approx 1$. On the other hand, for small Eo_D, the critical gas velocity is scaled with $(\sigma/\rho_G D)^{0.5}$ and is expected to increase with reducing the pipe diameter. It corresponds to a critical gas Weber number $(\mathrm{We}_G)_{\mathrm{crit}} = \rho_G U_{GS}^2 D/\sigma \approx 40$. In air-water systems, the capillary effect becomes important for $D < 1$ cm.

In Fig. 7, Eq. (12) corresponds to boundary 2 and is shown to predict reasonably the boundary between stratified wavy flow and annular flow in pipe diameters ranging between $0.6 < D < 2.5$ cm (see also Brauner and Moalem Maron, 1991, 1992, 1993, 1994). However, applying this criterion to the present test case of $D = 1$ mm ($\mathrm{Eo}_D = 0.02$) would suggest that the transition to annular flow occurs at $U_{GS} = 45$ m/s, which overpredicts the experimental transition. It is of interest to note that the KH stability criterion also overpredicts the transition at large Eo_D systems, as shown by boundary 2 in Fig. 9.

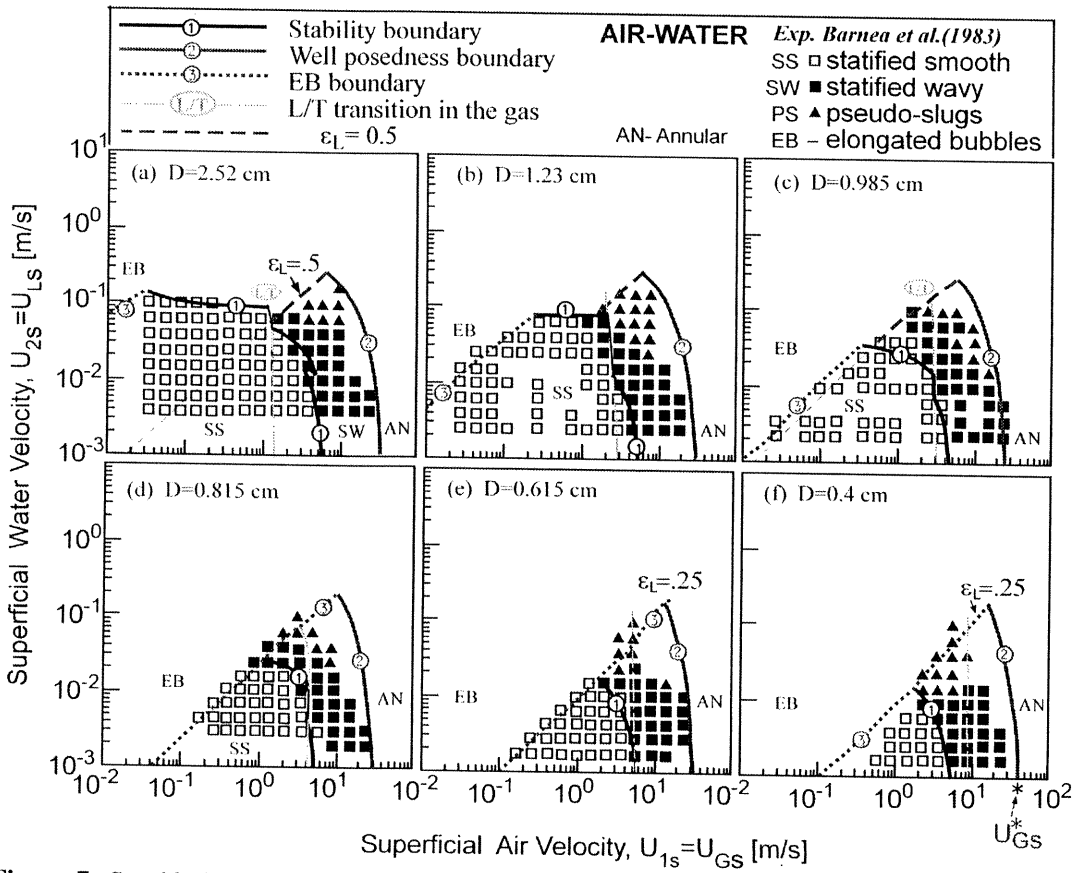

Figure 7 Stratified flow region: effect of pipe diameter.

6.2 *Drop entrainment*

The annular film is formed due to impingement of liquid drops, which are entrained from the wavy liquid interface. The drop breakage is due to the inertia of the fast gas phase (and not necessarily due to the turbulence in the gas phase). The inertia force is proportional to the initial velocity difference between the liquid and the gas stream, $\Delta U_G = U_G - U_L$ (in many practical applications, $U_G \gg U_L$, hence $\Delta U_G \approx U_G$). The critical Weber number for drop breakage can be related to the maximal drop size by the following empirical correlation (Brodkey 1969):

$$\mathrm{We}_{\mathrm{crit}} = \frac{\rho_G \Delta U_G^2 d_{\max}}{\sigma} = 12\left(1 + 1.077\mathrm{On}^{1.6}\right) \quad \mathrm{On} = \frac{\mu_L}{\sqrt{\rho_L d_{\max} \sigma}} \tag{13}$$

or

$$\left(\tilde{d}_{\max}\right)_o = \left(\frac{d_{\max}}{D}\right)_o = 12\left(1 + 1.077\mathrm{On}^{1.6}\right)\mathrm{We}_G^{-1}$$
$$\mathrm{We}_G = \frac{\rho_G \Delta U_G^2 D}{\sigma} \tag{14}$$

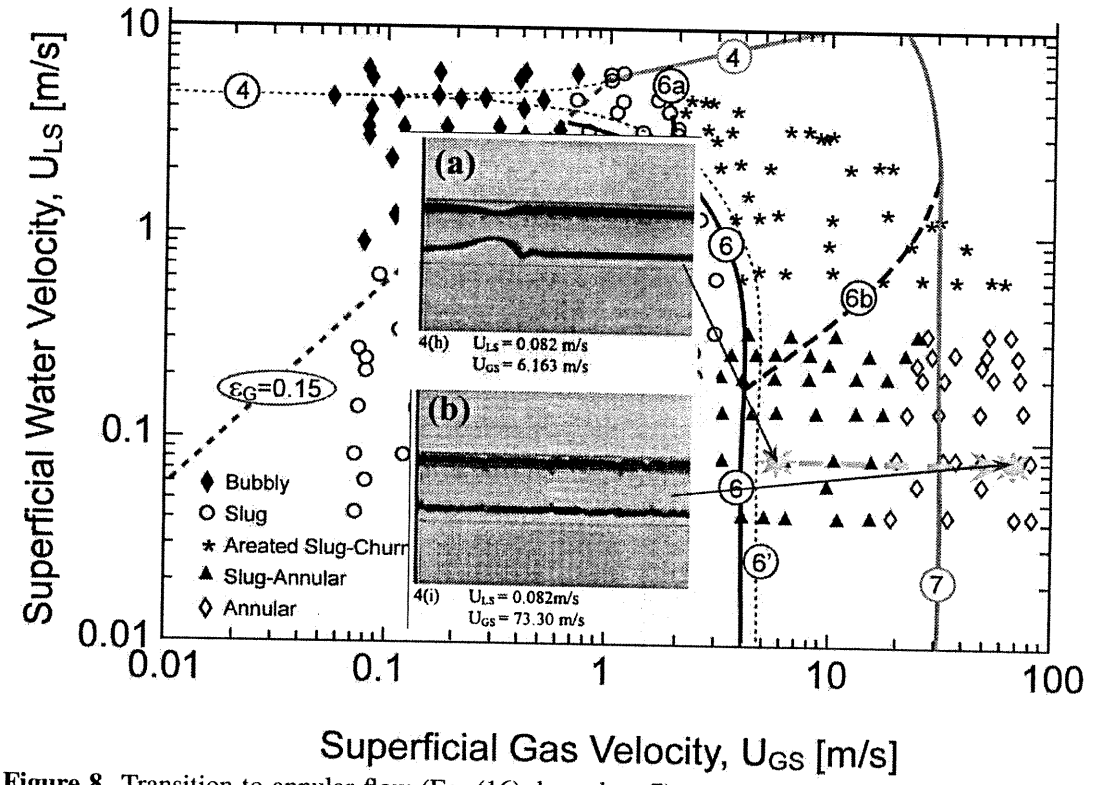

Figure 8 Transition to annular flow (Eq. (16), boundary 7).

The Ohnesorge number (On) in Eq. (13) accounts for the increase of the critical Weber number for the breakage of drops of highly viscous liquids. Although more sophisticated correlations were presented in the literature to account for the effects of drop velocity history prior to breakage (*e.g.*, Plich and Erdman 1987), correlation (13) is widely used to evaluate $d_{\max}$ in pneumatic atomization.

Similarly to the criterion used for modeling of the transition to fully dispersed flow (boundary 4), here too $d_{\max} \leq d_{\text{crit}}$ is used as a transitional criterion (see Eq. (3)). Obviously, the transition to annular flow due to impingement of drops on the pipe walls requires the presence of dispersive forces in the gas phase, namely, turbulence.

Different transition criteria evolve, depending on the relevant model for d_{crit}. For example, if the size of deformable drops $d_{c\sigma}$ represents the critical drop diameter, Eq. 3a, the following transitional criterion is obtained (E-model (Brauner 2003)):

$$\Delta U_G = U_G - U_L \geq 4.36 \left[\frac{\sigma \Delta \rho g \cos\beta}{\rho_G^2}\right]^{\frac{1}{4}} F(\text{On}) \tag{15}$$

where $F(\text{On}) = \left\{1 + 1.443(N_{vd}\cos\beta')^{0.4}\right\}^{0.5}$ and N_{vd} is the viscosity number of the dispersed (liquid) phase, $N_{vd} = \mu_L^4 \Delta\rho g/\left(\rho_L^2 \sigma^3\right)$. For air-water systems, $F(\text{On}) \approx 1$. It becomes significantly larger than 1 for high-viscosity liquids (typically, $\mu_L > 1\text{poise}$).

Note that when U_L is not negligible, the velocity difference can be obtained via an appropriate model (*e.g.*, a two-fluid model), which considers the fluid-separated flow geometry prior to the onset of drop entrainment (*e.g.*, stratified flow or annular flow).

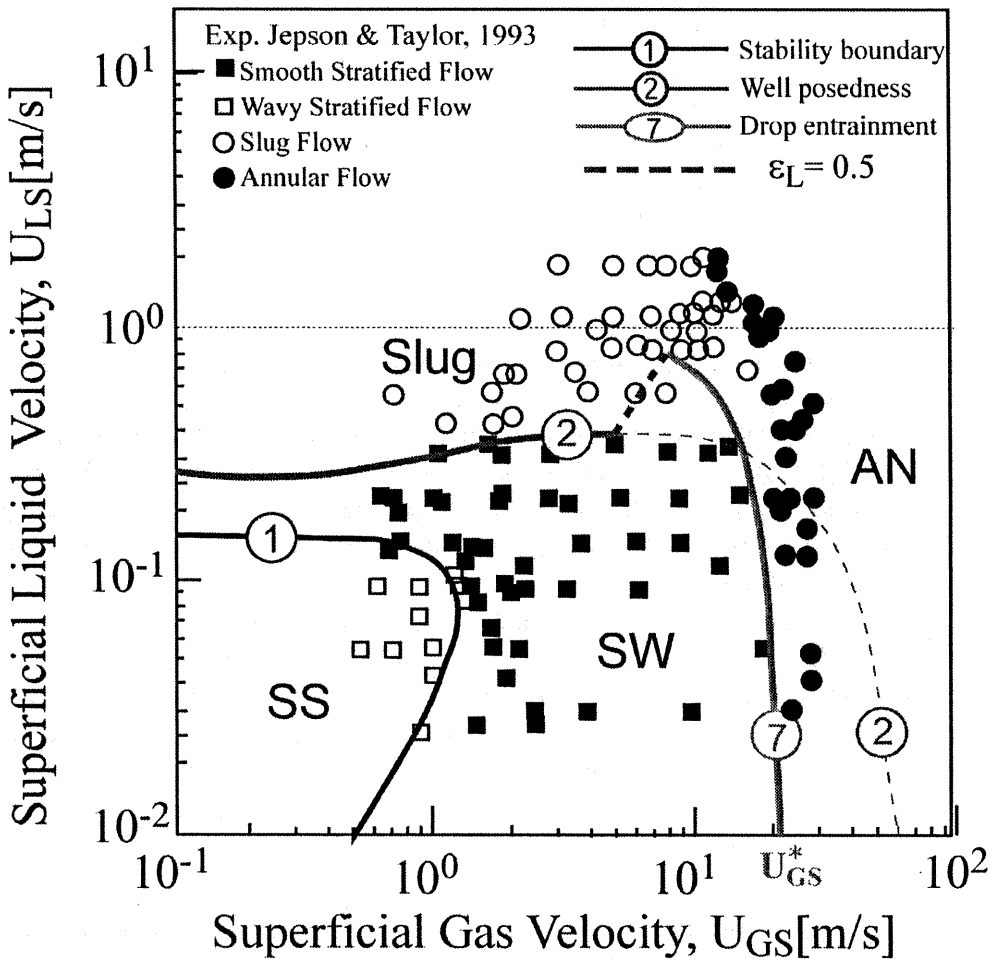

Figure 9 Flow patterns of atmospheric air-water flow in large-diameter pipe, D = 30 cm (data from Jepson and Taylor (1993)).

In systems of $\mathrm{Eo}_D < 0.2$, where the critical drop size is scaled with D(say, $d_{\mathrm{crit}} \simeq 0.5D$), the following transitional criterion is obtained (E1-model):

$$\Delta U_G = U_G - U_L \geq 4.9 \left[\frac{\sigma}{\rho_G D}\right]^{0.5} F(\mathrm{On}) \quad \mathrm{Re}_G > 2100 \tag{16}$$

where $F(\mathrm{On}) = \left\{1 + 1.875(\mu_L^2/\rho_L D\sigma)^{0.8}\right\}^{0.5}$. The critical gas velocity is scaled with $(\sigma/\rho_G D)^{0.5}$ and is expected to increase with reducing the pipe diameter, similarly to the trend predicted by the KH instability criterion for low Eo_D systems (see Eq. (12)). However, the E1-model, Eq. (16), corresponds to a lower critical gas Weber number, $(\mathrm{We}_G)_{\mathrm{crit}} = \rho_G U_{GS}^2 D/\sigma = 24$, compared to that implied by the KH model, $(\mathrm{We}_G)_{\mathrm{crit}} = 40$. Applying this criterion to the present test case of $\mathrm{Eo}_D = 0.02$ yields boundary 7 in Fig. 8, which is in reasonable agreement with the data.

It is worth noting that in this particular case study (Fig. 8), the critical gas velocity corresponding to boundary 7 approximately coincides with $\mathrm{Re}_G = 2100$ and thus with

the transition to turbulent flow (which is a necessary condition for the formation of the annular film due to drop impingement). However, in tube diameters smaller than 1 mm, boundary 7 for atmospheric air-water systems is in fact constrained by the condition $\mathrm{Re}_G > 2100$, implying that the critical gas velocity would then be proportional to D^{-1}. It is also worth mentioning that the turbulence intensity along boundary 7 in Fig. 8 is still too low to disperse the liquid into stable drops by the momentum of the turbulent eddies (Eq. (2)). The latter is met for $U_{GS} > 135$ m/s, where mist flow may be expected.

For air-water flow in large-diameter tubes, where Eq. (15) is applicable, the critical gas superficial velocity predicted by Eq. (15) is $U_{GS} = 20.35$ m/s (independent of the tube diameter). The application of this model to a large pipe diameter ($D =$ 30 cm) is shown in Fig. 9, indicating a much better agreement with the data of stratified/annular transition then that predicted by the inviscid KH stability criterion (boundary 2). Note that the gas and liquid velocity needed for applying the transition criteria were calculated using the two-fluid model presented in Ullmann and Brauner (2006). However, it is worth emphasizing that for horizontal pipes, Eq. (15) is applicable only in case $d_{\mathrm{crit}} = d_{c\sigma} < d_{cb}$.

For horizontal air-water flow in much larger pipe diameters ($D > 2.2$ m), the relevant critical drop diameter is $d_{\mathrm{crit}} = d_{cb} < 0.1D$ (given by Eq. (3c)). This indicates that for the establishment of the annular film in such large pipes, the turbulence in the gas phase should be further increased to overcome the settlement of the water drops due to gravity. In this case, boundary 7 is represented by the following condition:

$$U_G^6 \Delta U_G^2 \geq \frac{8}{9} \frac{\Delta\rho}{\rho_G^2} \frac{\sigma (g \cos\beta)^3 D^2}{f^2} \left(1 + 1.077\mathrm{On}^{1.6}\right) \tag{17a}$$

which for $U_G \gg U_L$ predicts that the critical gas velocity increases again with the tube diameter ($U_{GS} \propto D^{0.32}$, as f is dependent on Re_G). On the other hand, in horizontal systems where $d_{\mathrm{crit}} = d_{cb} > 0.1D$ (namely, the second expression in Eq. (3b) is valid), boundary 7 is represented by

$$U_G^2 \Delta U_G^2 \geq 32 \frac{\Delta\rho}{\rho_G^2} \frac{\sigma g \cos\beta}{f} \left(1 + 1.077\mathrm{On}^{1.6}\right) \tag{17b}$$

Here again, a very mild effect of the tube diameter is predicted (for $f = 0.046/\mathrm{Re}_G^{0.2}$, $U_{GS} \propto D^{0.053}$).

6.3 *Wave bridging*

The gas flow rate is sufficiently high to avoid wave bridging of the annular film and the formation of liquid slugs. Under such conditions, stable annular flow can be maintained. Favorable wave bridging conditions may be associated with an average holdup of $\varepsilon_L^{\mathrm{crit}} \geq 0.4 \div 0.5$. The liquid holdup can be calculated by applying an annular flow model. For small-diameter pipes and phases' flow rates, where the flows are laminar, the exact solution for annular flow (*e.g.*, Ullmann and Brauner 2004) is applicable. Using this model yields

$$U_{GS} \geq \tilde{\varepsilon}\left[\tilde{\varepsilon}\frac{\mu_L}{\mu_G} + 2\right] U_{LS} \quad \tilde{\varepsilon} = \frac{1 - \varepsilon_L^{\text{crit}}}{\varepsilon_L^{\text{crit}}} \tag{18}$$

Line 8 in Fig. 1 corresponds to this boundary with $\varepsilon_L^{\text{crit}} = 0.4$. As shown in the figure, in the region where $\varepsilon_L^{\text{crit}} = 0.4$, slug/annular flow was observed in the experiments.

6.4 *Wall wetting due to wave-induced secondary flows*

In the stratified wavy regime, the interface curvature is dominated by the wave phenomena and the resulting secondary flows. Possible mechanisms suggested in the literature include dragging of the liquid by gas secondary flows and/or pumping action due to lateral pressure gradient induced by the waves (see discussion in Ullmann and Brauner 2006). The shape of the interface can be practically represented in terms of the wetting angle, ϕ_0 and ϕ^*, that determines the interface curvature (see Fig. 10). The liquid holdup is given by

$$\varepsilon_L = \frac{1}{\pi}\left\{\phi_0 - \frac{1}{2}\sin(2\phi_0) - \frac{\sin^2\phi_0}{\sin^2\phi^*}\left[\phi^* - \pi - \frac{1}{2}\sin(2\phi^*)\right]\right\} \tag{19}$$

On the basis of a database of measured holdup (ε_L) and wetted perimeter (ϕ_0) in gas-liquid systems, a semiempirical correlation has been obtained for ϕ^* in the stratified wavy regime (Ullmann and Brauner 2006):

$$\phi^* = \pi + 2\,tg^{-1}Z; \quad Z = 57.2\left|\frac{\tau_G}{(\rho_L - \rho_G)\,g\cos\beta D}\frac{U_L}{U_G}\right|^{0.5}\tilde{S}_i \tag{20}$$

where $U_{L,G}$ are the liquid and gas average velocities and $\tilde{S}_i = S_i/D$ is the dimensionless interface perimeter. The derivation of this relation is based on the assumption that the interface curvature increases with the momentum of the secondary

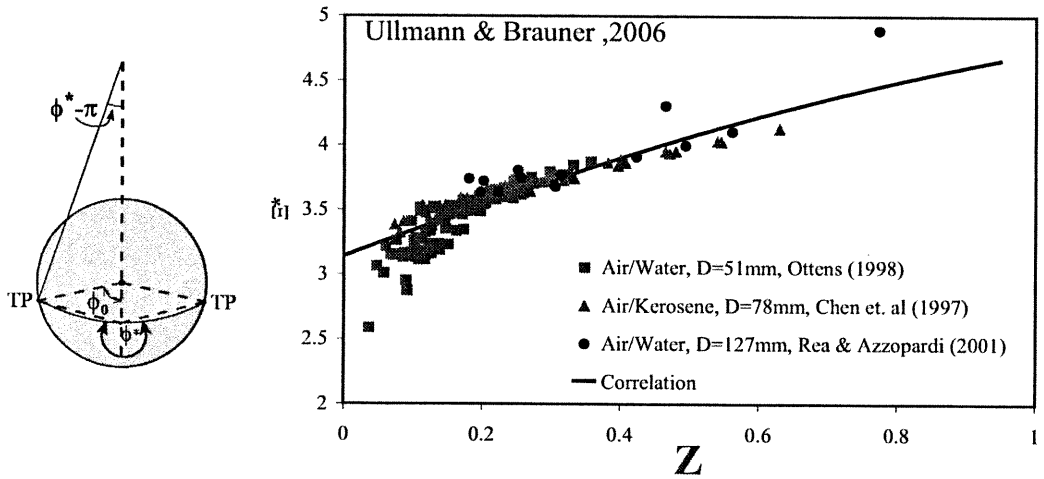

Figure 10 Experimental correlation for the interface curvature in wavy stratified gas-liquid flow (Eq. (18)).

flows (of the order of the shear velocity, $u^* = \sqrt{\tau_G/\rho_G}$) acting against the gravity restoring force, $(\rho_L - \rho_G)\, g \cos\beta D$. The values predicted for ϕ^* by this correlation are compared with experimental data in Fig. 10.

The validity of Eq. (20) is demonstrated by the favorable agreement with an additional independent data set obtained in a large-diameter tube of $D = 5''$ (Rea and Azzopardi 2001), which represents extrapolation to a much larger pipe diameter than that included in the original database. Equation (20) provides a closure relation for the interface curvature that can be combined with a two-fluid (TF) model to predict the stratified flow characteristics in the stratified wavy regime. Note that applying Eq. (20) to the test case of a 1-mm pipe also involves extrapolation, but this time to a smaller pipe diameter than that included in the database.

Figure 11 demonstrates the effect of pipe diameter on the predicted interface curvature and wetted perimeter for a relatively high gas flow rate (U_{GS} = 30 m/s) and a relatively low liquid flow rate (U_{LS} = 0.01 m/s) predicted by the TF model for stratified wavy flow (Ullmann and Brauner 2006). As shown, the extent of wall wetting (and curvature) increases with reducing the pipe diameter, and for the test case of a 1-mm pipe, an annular flow structure is practically approached ($\phi^* \to 2\pi$, $\phi_0 \to \pi$).

6.5 *Surface tension and wall wetting effects*

In low Eo_D systems, surface tension and the fluid/wall wetting characteristics become important. The wetting liquid tends to spread over the tube wall. In extreme cases of ideal wetting of the liquid phase and small Eo_D, the liquid can completely wet the wall surface and thus form an annular flow structure, even under conditions of negligible inertial effects in the flow (the latter are involved in the above-mentioned mechanisms).

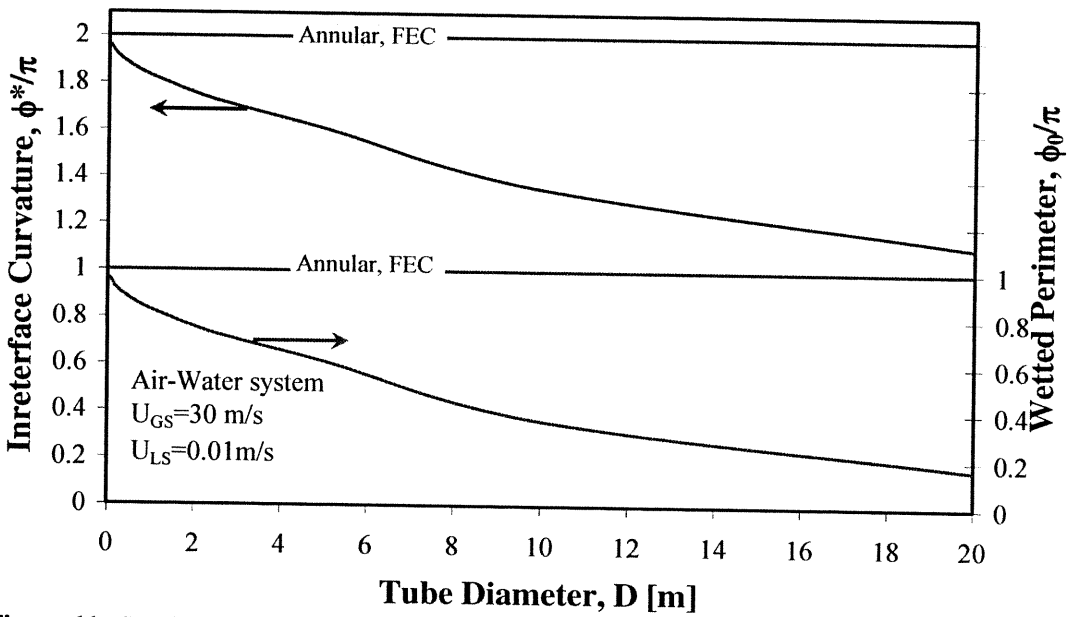

Figure 11 Stratified flow structure in case of wall wetting due to wave-induced secondary flows: effect of tube diameter.

In fully developed laminar separated flows, and in the absence of interfacial waves, the interface shape depends on the Eo_D number, the fluid/wall contact angle, α, and the *in situ* holdup (Brauner *et al.* 1996a, Gorelik and Brauner 1999).

In the extreme of a gravity-dominated system ($Eo_D \gg 1$), the interface is practically plane ($\phi^* \to \pi$) independently of the holdup. On the other extreme of a surface tension–dominated system ($Eo_D \ll 1$), the interface curvature is given by $\phi^* = \phi_0 - \alpha + \pi$, with $\phi_0 + \pi < \phi < \phi^*$ (Brauner *et al.* 1996a, Gorelik and Brauner 1999). As shown in Fig. 12, the case of $\alpha = 0$ (the wall is ideally wetted by the heavy phase) corresponds to fully eccentric core of the light phase, $\phi^* = 2\pi$, whereas with $\alpha = \pi$, the solution obtained corresponds to a fully eccentric core of the heavy phase, $\phi^* = 0$.

Figure 12 demonstrates the effect of the Eo_D number and liquid holdup on the wetting of the pipe wall for the case of $\alpha = 0$. The ϕ_0 and corresponding ϕ^* were obtained by the model presented in Brauner *et al.* (1996a). The fraction of the wall wetted increases with reducing Eo_D and with the liquid holdup. Obviously, the lowest wall wetting corresponds to a gravity-dominated system, $Eo_D \to \infty$, where the interface is plane. On the other extreme of $Eo_D \to 0$, the wall is completely wetted by the liquid, and the flow geometry is of a fully eccentric core-annular flow. The figure also shows the results obtained for the flow of air-water and for refrigerant 410a vapor-liquid flow in a 1-mm pipe.

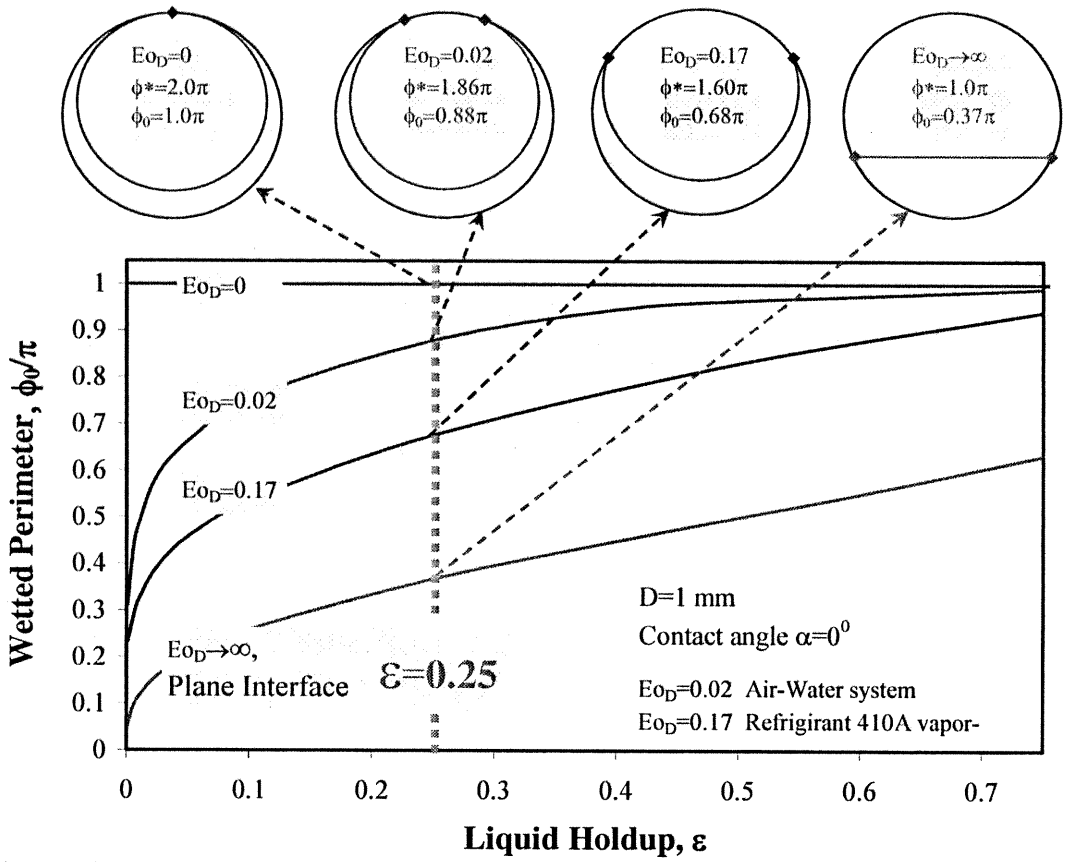

Figure 12 Stratified flow structure due to surface tension for ideally wetting liquid: effect of liquid holdup.

In gas-liquid systems, the liquid is generally the wetting phase. Therefore, in the case of $\alpha \rightarrow 0$, an annulus of the liquid phase is to be considered as the prevailing configuration in low-Eo_D systems at low flow rates. This configuration replaces the stratified flow with a plane interface, which is observed at low flow rates in large Eo_D (gravity-dominated) systems.

The flow structures for liquid holdup of 0.25 obtained for the various Eo_D are also depicted in Fig. 12. It is shown that for the air-water test case considered in this study, the wall wetting is almost complete already with this rather low water holdup. Visual observations of such a flow, for this and higher holdups, would most probably lead to a classification of the flow structure as annular.

7. EXISTENCE OF STRATIFIED FLOW IN MINITUBES

The stratified flow regime was not reported in the flow pattern map of Triplett *et al.* (1999). The question is, What are the flow patterns that can be expected at lower liquid flow rates than those included in Fig. 1?

Figure 13 shows the predicted stratified-smooth/wavy (SS/SW) transition boundary (line 1) calculated based on the viscid KH stability criterion (Brauner and Moalem Maron 1991, 1993, 1994). It is worth noting that as the flow in the gas (and liquid) phase is laminar in this range, the wave-sheltering mechanism is negligible (Brauner

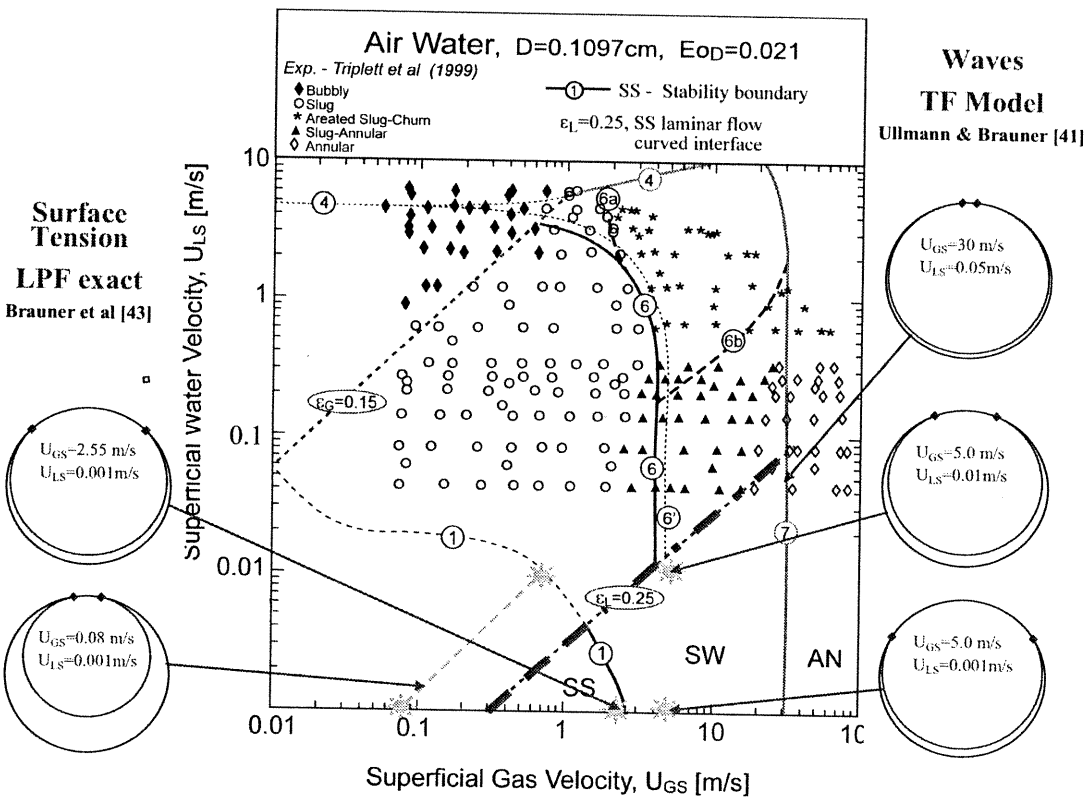

Figure 13 Stratified flow region and the corresponding predicted flow structure.

and Moalem Maron 1994) and therefore not considered. The locus of liquid holdup of 0.25 in smooth stratified flow is also indicated in the figure. It has been obtained by the exact solution for laminar stratified flow in the 1 mm pipe (Brauner *et al.* 1996b, Ullmann *et al.* 2006) when applied for interface shape obtained for $Eo_D = 0.02$ and $\alpha = 0$ (see Fig. 12). As demonstrated in the figure, in the region below boundary 1 and for liquid holdup higher then 0.25, the wall is practically wetted by the water, and the flow pattern would not be classified as stratified flow. Whether annular flow may exist in this region depends on the gas core stability. Capillary instability of the gas core may result in bubbly flow or elongated bubble flow. These flow patterns were reported in this region in slightly larger-diameter pipes (see Fig. 6 and Brauner (1990)). On the other hand, for liquid holdup lower than 0.25 (still in the SS region, below boundary 1), a significant part of the wall perimeter is not wetted by the liquid. Therefore the flow structure actually corresponds to stratified flow. For higher contact angles ($\alpha > 0$) and/or lower surface tension, the stratified flow structure is expected to be even more pronounced. Indeed, in the range of liquid and gas flow rates corresponding to the SS and SW regions in Fig. 13, stratified flow was identified in some experimental studies of air-water flow in minichannels of D = 1–2 mm (Damianides and Westwater 1988, Brauner and Moalem Maron 1993). However, in the SW region, the predicted liquid layer (film) thickness is very thin and may rupture to form rivulets and drops. The film rupture is dependent on the wall conditions (*i.e.*, roughness, scales) and wetting phenomena.

At higher gas flow rates, in the region predicted to be SW (beyond boundary 1), the wave-induced secondary flows the wetting mechanism prevail. The flow structure predicted in this region is again dependent on the holdup. However, with the extended wall wetting expected in this region, the flow characteristics are practically similar to that of annular flow (except at extremely low liquid flow rates).

8. CONCLUSIONS

The characterization of small-diameter pipes has been examined from the point of view of two-phase flow pattern maps. Various mechanisms involved in flow pattern transitions have been reviewed, and the relevant dimensionless variables have been identified.

The Eo_D number was shown to play a major role in determining the relevant characteristic length in dispersed flows and the wall wetting effects in separated flows. $Eo_D \sim 0.2$, namely, $\Delta\rho g D^2/\sigma \leq 1.6$, can be considered as a characteristic threshold value for switching to different modeling of flow pattern transitions that are valid in minichannels. It corresponds to D = 0.35 mm for air-water systems and $D \sim 1$ mm for refrigerant vapor-liquid systems (*e.g.*, refrigerant 134a at 5–15 bar). The models suggested in this study were found to predict reasonably the flow pattern transitions for the test case for of air-water flow in 1-mm pipe.

The annular configuration in small Eo_D systems can be obtained due to surface tension and fluid/wall wetting characteristics and/or due to inertial effects. It is important to identify the prevailing wall wetting mechanism that leads to annular flow as the different mechanisms are associated also with different modeling of pressure drop, heat, and mass transfer.

With reducing the pipe diameter, the stratified flow region shrinks and may be limited to only a small region of very low liquid flow rates (and relatively high gas flow rates). In the flow rate range where stratified flow may still exist, analysis of the predicted flow structure indicates that the distinction between stratified flow (curved interface) and annular flow is ambiguous. However, from the practical point of view of the transport phenomena involved, the flow structure can be considered as annular.

Finally, it is worth noting that in the case of noncircular tubes, the Eo_D is often defined by replacing D with the hydraulic diameter. However, the hydraulic diameter may not correctly represent the relative significance of gravity and surface tension forces in the system. For instance, in horizontal square channels (channel height H and width W), the gravity force is scaled by $\Delta\rho g H$, while the surface tension force is scaled by σ/W. Accordingly, a more appropriate definition of the characteristic system Eotvos number would be $\mathrm{Eo} = \Delta\rho g H W/\sigma$, which would suggest that channels of high aspect ratios are more gravity dominated than implied by their hydraulic diameter.

NOMENCLATURE

C_K	constant, Eq. (6)	
C_1	constant, Eq. (12)	
d_{cb}	characteristic size of floating droplet/bubble	m
$d_{c\sigma}$	characteristic size of deformable droplet/bubble	m
D	diameter	m
D_h	hydraulic diameter	m
Eo_D	system Eotvos number	
f	friction factor	
Fr	Froude number	
g	gravitational acceleration	$\mathrm{m/s^2}$
H	channel height	m
h	liquid layer thickness	m
k	wave number	$\mathrm{m^{-1}}$
L_{pipe}	pipe length	m
N_{vd}	viscosity number	
On	Ohnesorge number	
Q	flow rate	$\mathrm{m^3/s}$
Re	Reynolds number	
S	perimeter	m
U	velocity	m/s
u^*	frictional velocity	m/s
W	channel width	m
We	Weber number	
Z	parameter, Eq. (20)	
α	contact angle	
β	inclination	rad
$\Delta\rho$	density difference	$\mathrm{kg/m^3}$
ε	phase holdup (or void fraction)	

μ	viscosity	kg/s/m
ρ	density	kg/m^3
σ	surface tension	N/m
τ	shear stress	N/m^2
$\phi*$	interface curvature	rad
ϕ_0	liquid phase wetted perimeter	rad
c	continuous	
crit	critical	
d	dispersed	
G, GS	gas phase, superficial	
L, LS	liquid phase, superficial	
Lf	liquid film	
m	mixture	
i	interfacial	
max	maximal	
E	dense	
o	dilute	
$\tilde{}$	dimensionless (scaled by D)	

REFERENCES

Barajas, A. M., and Panton, R. L. (1993), The Effect of Contact Angle on Two-Phase Flow in Capillary Tubes, *Int. J. Multiphase Flow*, **19**, 337–346.

Barnea, D., and Brauner, N. (1985), Hold-up of the Liquid Slug in Two Phase Intermittent Flow, *Int. J. Multiphase Flow*, **11**, 43–49.

Barnea, D., Luninski, Y., and Taitel, Y. (1983), Flow Pattern in Horizontal and Vertical Two Phase Flow in Small Diameter Pipes, *Can. J. Chem. Eng.*, **61**, 617–620.

Biswas, J., and Greenfield, P. F. (1985), Two-Phase Flow through Vertical Capillaries—Existence of a Stratified Flow Pattern, *Int. J. Multiphase Flow*, **11**, 553–563.

Brauner, N. (1990), On the Relation between Two-Phase Flow under Reduced Gravity and Earth Experiment, *Int. Commun. Heat Mass Transfer*, **17**, 271–282.

Brauner, N. (2001), The Prediction of Dispersed Flows Boundaries in Liquid-Liquid and Gas-Liquid Systems, *Int. J. Multiphase Flow*, **27**, 911–928.

Brauner, N. (2003), Liquid-Liquid Two-Phase Flow Systems, in *Modeling and Experimentation in Two-Phase Flow Phenomena*, V. Bertola (ed.), Springer, New York.

Brauner, N., and Moalem Maron, D. (1991), Analysis of Stratified/Non-stratified Transitional Boundaries in Horizontal Gas-Liquid Flows, *Chem. Eng. Sci.*, **46**, 1849–1859.

Brauner, N., and Moalem Maron, D. (1992), Identification of the Range of Small Diameter Conduits Regarding Two-Phase Flow Patterns Transitions, *Int. Commun. Heat Mass Transfer*, **19**, 29–39.

Brauner, N., and Moalem Maron, D. (1993), The Role of Interfacial Shear Modeling in Predicting the Stability of Stratified Two-Phase Flow, *Chem. Eng. Sci.*, **8**, 2867–2879.

Brauner, N., and Moalem Maron, D. (1994), Stability of Two-Phase Stratified Flow as Controlled by Laminar Turbulent Transition, *Int. Commun. Heat Mass Transfer*, **21**, 65–74.

Brauner, N., and Ullmann, A. (2004), Modeling of Gas Entrainment from Taylor Bubbles: Slug Flow, *Int. J. Multiphase Flow*, **30**, 273–290.

Brauner, N., Rovinsky, J., and Moalem Maron, D. (1996a), Analytical Solution for Laminar-Laminar Two-Phase Stratified Flow in Circular Conduits, *Chem. Eng. Commun.*, **141–142**, 103–143.

Brauner, N., Rovinsky, J., and Moalem Maron, D. (1996b), Determination of the Interface Curvature in Stratified Two-Phase Systems by Energy Considerations, *Int. J. Multiphase Flow*, **22**, 1167–1185.

Brauner, N., Moalem Maron, D., and Rovinsky, J. (1998), Two-Fluid Model for Stratified Flows with Curved Interfaces, *Int. J. Multiphase Flow*, **24**, 975–1004.

Brodkey, R. S. (1969), *The Phenomena of Fluid Motions*, Addison-Wesley, Reading, MA.

Chen, W. L., Twu, M. C., and Pan, C. (2002), Gas-Liquid Two-Phase Flow in Micro-Channels, *Int. J. Multiphase Flow*, **28**, 1235–1247.

Cheng, L. X., and Mewes, D. (2006), Review of Two-Phase Flow and Flow Boiling of Mixtures in Small and Mini Channels, *Int. J. Multiphase Flow*, **32**, 183–207.

Damianides, C. A., and Westwater, J. W. (1988), Two-Phase Flow Patterns in a Compact Heat Exchange and in Small Tubes, *Proc. UK National Heat Transfer Conf.*, 1257–1268.

Fukano, T., and Kariyasaki, A. (1993), Characteristic of Gas-Liquid Two-Phase Flow in a Capillary Tube, *Nucl. Eng. Design*, **141**, 59–68.

Ghiaasiaan, S. M., and Abdel-Khalik, S. I. (2001), Two-Phase Flow in Micro-Channels, *Adv. Heat Transfer*, **34**, 145–254.

Gorelik, D., and Brauner, N. (1999), The Interface Configuration in Two-Phase Stratified Flow, *Int. J. Multiphase Flow*, **25**, 877–1007.

Hetstroni, G., Mosyak, A., Pogrebnyak, E., and Yarin, L. P. (2005), Fluid Flow in Micro-Channels, *Int. J. Heat Mass Transfer*, **48**, 1982–1998.

Hinze, J. O. (1955), Fundaments of the Hydrodynamic Mechanism of Splitting in Dispersion Processes, *AIChE J.*, **1**, 289–295.

Jepson, W. P., and Taylor, R. E. (1993), Slug Flow and Its Transitions in Large Diameter Horizontal Pipes, *Int. J. Multiphase Flow*, **22**, 411–426.

Kandlikar, S. G. (2001), Two-Phase Flow Pattern Pressure Drop and Heat Transfer during Boiling in Mini-Channel and Micro-Channel Flow Passages of Compact Evaporators, *Proc. of the 3rd Int. Conf. on Compact Heat Exchangers and Enhancement Technology for Process Industries*, 319–334.

Kandlikar, S. G. (2002), Fundamental Issues Related to Flow Boiling in Mini-Channels and Micro-Channels, *Exp. Thermal Fluid Sci.*, **26**, 889–407.

Kew, P. A., and Cornwell, K. (1997), Correlation for the Prediction of Boiling Heat Transfer in Small Diameter Channels, *Appl. Thermal Eng.*, **17**, 705–715.

Lowe, D. C., and Rezkallah, K. S. (1999), Flow Regime Identification in Microgravity Two-Phase Flows Using Void Fraction Signals, *Int. J. Multiphase Flow*, **25**, 433–457.

Mehendale, S. S., Jacobi, A. M., and Ahah, R. K. (2000), Fluid Flow and Heat Transfer at Micro- and Meso-Scales with Application to Heat Exchanger Design, *Appl. Mech. Rev.*, **53**, 175–193.

Plich, M., and Erdman, C. A. (1987), Use of Breakup Time Data and Velocity History Data to Predict the Maximum Size of Stable Fragments for Acceleration Induced Breakup of Liquid Drop, *Int. J. Multiphase Flow*, **13**, 741–757.

Rea, S., and Azzopardi, B. J. (2001), The Split of Horizontal Stratified Flow at Large Diameter T-Junction, *Trans. IChemE*, **79**, 470–476.

Rezkallah, K. S. (1996), Weber Number Based Flow-Pattern Maps for Liquid-Gas Flows at Microgravity, *Int. J. Multiphase Flow*, **22**, 1265–1270.

Serizawa, A., Feng, Z. P., and Kawara, Z. (2002), Two-Phase Flow in Micro-Channels, *Exp. Thermal Fluid Sci.*, **26**, 703–714.

Suo, M., and Griffith, P. (1964), Two-Phase Flow in Capillary Tubes, *J. Basic Eng.*, **86**, 576–582.

Taitel, Y., and Dukler, A. E. (1976), A Model for Prediction Flow Regime Transition in Horizontal and Near Horizontal Gas-Liquid Flow, *AIChE J.*, **22**, 47–55.

Thome, J. R. (2006), State of the Art Overview of Boiling and Two-Phase Flows in Microchannels, *Heat Transfer Eng.*, **27**, 4–19.

Triplett, K. A., Ghiaasiaan, S. M., Abdel-Khalik, S. I., and Sadowski, D. L. (1999), Gas-Liquid Two-Phase Flow in Micro-Channels, Part 1: Two-Phase Flow Patterns, *Int. J. Multiphase Flow*, **25**, 377–394.

Ullmann, A., and Brauner, N. (2004), Closure Relations for the Shear Stresses in Two-Fluid Models for Core-Annular Flow, *Multiphase Sci. Technol.*, **16**, 355–387.

Ullmann, A., and Brauner, N. (2006), Closure Relations for Two-Fluid Models for Two-Phase Stratified Smooth and Stratified Wavy Flows, *Int. J. Multiphase Flow*, **32**, 82–105.

Ullmann, A., Goldstein, A., and Brauner, N. (2006), Gas-Liquid and Liquid-Liquid Stratified Flows: Exact Analytical Solutions and Mechanistic Models, *IFFM Trans. Fluid Flow*, **32**, 82–105.

Wallis, G. B. (1969), *One Dimensional Two-Phase Flow*, McGraw-Hill, New York.

Watel, B. (2003), Review of Saturated Flow Boiling in Small Passages of Compact Heat Exchangers, *Int. J. Thermal Sci.*, **42**, 107–140.

Wilmarth, T., and Ishii, M. (1994), Two-Phase Flow Regimes in Narrow Rectangular Vertical and Horizontal Channels, *Int. J. Multiphase Flow*, **37**, 1749–1758.

Zukoski, E. E. (1966), Influence of Viscosity, Surface Tension, and Inclination Angle on Motion of Long Bubbles in Closed Tubes, *J. Fluid Mech.*, **25**, 821–837.